Modified Generalized Maxwell Model for Hysteresis Behavior of Elastomeric Dampers

Christos A. Basagiannis[1] and Martin S. Williams[2]

[1]Corresponding author, Department of Engineering Science, University of Oxford, Oxford, United Kingdom. Email: chrisbasa2331@gmail.com

[2]Department of Engineering Science, University of Oxford, Oxford, United Kingdom. Email: martin.williams@eng.ox.ac.uk

ABSTRACT

A constitutive model is presented for the hysteretic behavior of elastomeric material, called the Modified Generalized Maxwell Model (MGMM). A new force-displacement relationship which describes the well known Generalized Maxwell Model (GMM) is also proposed in this study, and forms the basis for the MGMM. This relationship can be used regardless the number of Maxwell elements. The damper was first characterised using terms of Visco-Elastic (VE) material, determining its shear storage modulus and loss factor for a range of cyclic tests. This led not only to an understanding of how the main mechanical properties of the damper change when strain amplitude, frequency, and temperature change, but also to a more detailed understanding of how the hysteresis shape of the material change along the alteration of these parameters. The final model was calibrated using test data obtained from sweep amplitude tests over a range of frequencies, and ambient temperatures and was able to accurately predict the dynamic performance of the dampers.

INTRODUCTION

Passive energy dissipation devices have the ability to improve the seismic behavior of buildings(Makris and Constantinou 1991; Shen and Soong 1995; Soong and Dargush 1997; Fan 1998; Lee 2003; Vargas and Bruneau 2007; Shrimali et al. 2015) by reducing drift, force and deformation

demands on the structural elements, which are responsible for providing lateral load resistance, in addition to reducing velocity and acceleration demands on non-structural components(Karavasilis et al. 2012). This paper focuses on the evaluation of the hysteresis behavior of two Elastomeric Dampers (EDs), developed by TARRC (the Tun Abdul Razak Research Center, UK).

Elastomers, like many other polymers, show viscoelastic properties, and hence highly depend on the strain amplitude, frequency, and ambient temperature. However, (Lee 2003) showed that elastomeric dampers are less sensitive to frequency compared to conventional viscoelastic materials, a fact which makes them even more effective. Moreover, a distinct feature of the hysteresis loops of elastomers is that softening at a small strain amplitude and hardening at a relatively large strain amplitude may occur in the amplitude range of practical interest (Sause et al. 2007). Similar softening-hardening hysteresis behavior was observed for elastomeric dampers (Sause et al. 2007), and for high damping rubber base isolators (Taniwangsa and Kelly 1996; Aiken 1997). Another interesting characteristic of the elastomeric materials, known as the Mullin's effect, is the softening of the material under the first few cycles of deformation, after which the stress-strain behavior approaches a steady state (Hepburn and Reynolds 1979). The main properties of the elastomers can be summarized as: exhibit VE behavior especially under relatively small strains, extremely high extensibility, complete recovery after removal of the imposed stress, and strain hardening at relative large strains. These are advantageous for passive dissipation devices since, even after strong earthquakes, the elastomeric dampers will not exhibit any damage or permanent deformation, resulting in more economical solutions.

Most elastomer applications for seismic protection of structures have been implemented for seismic isolated structures (Koh and Kelly 1990; Papoulia and Kelly 1994; Shrimali et al. 2015; Silwal et al. 2015) in the form of elastomeric bearings for base isolation. There are a few applications of VE dampers which were used retrofitting structures connecting the damper with the braces. The main target of the first implementations of the VE dampers were to reduce the wind induced vibrations. Therefore, one of the first applications of VE dampers was in the World Trade Center (1969) in order to reduce the acceleration levels due to wind (Mahmoodi et al. 1987). Hence, about

10000 VE dampers were installed in each tower from the 10th to the 110th floor. Their design was carried out in such a way to assist the steel frame mitigating the wind induced movement. They were located between the lower chords of the horizontal trusses and the the outer columns of the structure. The total achieved damping was calculated and found to be in the range of 2.5%-3% of critical. Seismic applications started a lot later, and more specifically in 1993 where the 13 story Santa County building in San Jose, CA, was decided to be retrofitted, since it was found that the viscous damping in the fundamental mode was less than 1% of critical. VE dampers were chosen as final solution, since they could provide increased damping for both frequent low-level ground shaking and strong ground motions. Two VE dampers were added to each building face per floor, increasing the fundamental damping to 17% of the critical. More recent applications of VE dampers connected with steel diagonal braces include the Beijing 7 Star Morgan Plaza Hotel C (China, Beijing) in 2007 where 108 viscous and viscoelastic dampers were added for both wind and earthquake protection, and the Hotel Stockton (USA, Stockton, CA), where a combination of both viscous and viscoelastic dampers were added to reduce the structure's response due to seismic loads (Kit Miyamoto and Lon M. Determan). Another different approach was followed by Rant D.R. (Pant et al. 2017), where a 110-story, 630 m mega-tall building was retrofitted with VE dampers, which replaced the coupling beams connecting the shear walls. The main concept behind this decision is that since the deflected shape of very tall buildings due to horizontal loads is similar to cantilever, rather than the shear deflection of moment resisting frames which consists the main resisting system of low-rise buildings. Hence, the whole dampers philosophy was adjusted as well. The dampers replaced about 60% of the diagonally reinforced concrete coupling beams of the original structure. The results showed that the peak inter-story drift ratios were reduced by up to 15% under the Maximum Considered Earthquake, and the peak floor accelerations by approximately 24%. One of the rare applications of rubber-like dampers connected with the surrounding structure with diagonal braces was carried out by Teramoto T. (Teramoto et al. 1996) on a 11 story, 44 m tall building. The main target of the added dampers was to reduce the vibrations due to both seismic loads and traffic motion since the building was close to subway lines. The results improved the building's performance

by reducing both the maximum accelerations and story drifts by approximately 20%. Another seismic retrofit was carried out in the Gentile-Fermi School in Fabriano, after the building suffered sufficient damage during an earthquake in the Umbria-Marche region (September 1997). A total of 33 elastomeric dampers were added at the second and the third floor of the building absorbing 50% of the input energy.

Numerous models have been proposed in order to simulate the hysteresis behavior of elastomeric materials as passive dissipative devices. Lee (2003) proposed rate-independent and rate-dependent models based on asymptotic functions, simulating softening and hardening behavior which the elastomer experiences, using second and third order polynomials. A linear dashpot was also added to the proposed model in order to take into account rate dependent effects. However, the results were not satisfactory for the entire range of frequencies which were used, while also some discrepancies were noticed between the experimental and analytical values regarding the equivalent shear modulus and especially the loss factor. Kästner et al. (2012) proposed a linear combination of rate independent and rate dependent components as a way of modelling the inelastic material behavior. Even though good results were achieved for relaxation and tensile tests, the comparison with cyclic loading showed that the model overestimates the hysteresis. Shen and Soong (1995) used Boltzmann's superposition principle (Ferry 1980). The model was only valid under the assumption of linearity, and limitations of frequency below 3Hz, and shear strain amplitude below 20%, where viscoelastic effects are dominant. Generalized Maxwell (or Kelvin) models (GMM) (McCrum et al. 1997; Karavasilis et al. 2011) and Fractional-Derivative models (Koh and Kelly 1990; Makris and Constantinou 1991) have been also proposed to capture rate dependent effects of passive dissipative dampers. The Bouc-Wen model has been also used (Constantinou and Tadjbakhsh 1985; Yu et al. 2016), especially in the case of elastomeric materials being used in base isolation. Petrone et al. (2004) proposed an assembly of springs, dashpots, and Coulomb friction sliders in order to represent the dynamic characteristics of elastomers in both in series and in parallel configuration. Comparison was made based on stiffness-frequency and damping-frequency terms. Jrad et al. (2013) used a non linear GMM for viscoelastic representation with

satisfying accuracy in frequency domain. He has also proposed a model which couples GMM with a friction model developed by Dahl (Dahl 1968), with promising results (Jrad et al. 2017) in an attempt to simulate elastomeric rotational joint behavior under harmonic loading. However, the conventional way of modeling elastomeric behavior, at least for design purposes, is the simpler one that FEMA (Prestandard 2000) proposes, where an equivalent stiffness and loss factor are assumed for the elastomer based on the natural frequency of the building. Moreover, Silwal et al. (2015) used a ViscousDamper material based on the Maxwell material property, in order to model elastomeric behavior as part of a hybrid passive damper.

To determine the main characteristics of elastomeric dampers as passive dissipation devices, shear storage modulus and shear loss factor (McCrum et al. 1997; Soong and Dargush 1997) should be obtained for a range of strain amplitude, rate of loading, and ambient temperature. These values usually form the basis to design a structure with dissipative systems in order to achieve an advanced performance level, which will lead the structure not only to be able to withstand strong earthquakes without severe damage, but also to maintain its functionality. In contrast, the common design approach prevents the structure from collapse, but at the same time energy dissipation is expected to occur in specially designed ductile plastic hinge regions of beams and columns bases. This design approach has been considered acceptable because of economic considerations provided, of course, that structural collapse is prevented and life safety is ensured (Constantinou et al. 1998). However, under large earthquakes the damage may not be restricted to the aforementioned regions, but can extend to the majority of the columns leading to permanent deformation in undesired locations with potential catastrophic and uneconomical results. Hence, structures are often desired to achieve a more advanced performance level even due to strong earthquakes, especially if these structures are defined as highly important, such as hospitals, schools, and museums.

This paper examines the effect of elastomeric materials when used as discrete dampers in the form of a layer bonded between two steel plates. The design philosophy is to implement the dampers throughout the height of the structure, with dampers inserted between the connection of additional diagonal braces and the middle of the beam of the upper floor. The dissipation mechanism is

triggered through shear deformation of the material, as the building moves due to dynamic loading.

A differential time-domain equation to accurately simulate the shear force-displacement behavior of the elastomer, based on the Generalized Maxwell Model (GMM), is presented here. Apart from the traditional characterization tests, sweep amplitude displacement tests at different frequencies were also carried out in order to form the basis of the data used to calibrate the model. Furthermore, an extension to the model is proposed in order to capture dynamic behavior of the damper under different ambient temperatures. Part of the proposed hysteresis model is a new equation which describes the force-displacement relationship of the GMM in the time domain for any given displacement and any given value, N, of the Maxwell elements which is updated for every time-step.

ELASTOMERIC DAMPER AND CHARACTERIZATION TESTS

Two elastomeric dampers were provided by the Tun Abdul Razak Research Centre (TARRC). They consist of a rubbery material, consisting of natural rubber, carbon black, and resin, bonded between steel plates.The cure for material test-pieces was 30 minutes at 150^{o}C. Material properties can be seen in Table 1.

Each of these dampers has overall dimensions of 260x260 mm^2, of which only 180x230 mm^2 corresponds to the elastomer's dimensions while the materials' thickness is 11.75 mm (fig.2). The 230 mm dimension coincides with the loading direction. For testing, each elastomeric damper was connected to additional steel plates, A (fig.1), which were connected to a stable reacting wall. The interior plate of the damper was connected to a plate, B (fig.1), which in turn enables connection to the actuator via a central plate , C (fig.1). The final configuration of the rig can be seen at Fig.1.

This arrangement allowed the two dampers to be tested simultaneously in shear in a symmetric arrangement. Loads were applied by a 100 kN servo-hydraulic actuator. A thermo-couple was also attached to the elastomer in order to measure the ambient temperature, and to capture any increase in temperature during the tests. It is well known that rubber-like materials exhibit non linear behavior that depends on strain amplitude, ambient temperature, loading frequency, and loading history (Lee 2003). Hence, the experimental tests were focused on verifying non linear dependence

159 on these parameters. Among these parameters, it is has been shown that strain dependence is the
160 most dominant factor (Papoulia and Kelly 1994; Lee 2003).

161 In order to investigate the effect of these parameters a series of tests was carried out based
162 on sinusoidal displacement histories at the EDs. In order to avoid large initial displacement and
163 velocity, ramping cycles were implemented, along with 18 full sinusoidal cycles. This process was
164 repeated for frequencies 0.25, 0.5, 1.0, 2.0, 3.0, and 4.0Hz, for strain amplitudes 10, 20, 30, 40,
165 and 50%, and for ambient temperatures 20, 25, 30, and 35°C. The maximum shear strain amplitude
166 was kept within 50%, to avoid any potential permanent damage, severe cracking, or debonding of
167 the elastomer.

Elevated temperature tests were achieved with the use of a heater, and a temperature control chamber, so that the target temperature was kept stable during the test. During testing it was noticed that after the first loading cycles, the hysteresis loops became more and more steady and approximately repeatable, corresponding to smaller and smaller stiffness degradation. Hence, in order to determine the mechanical properties of the dampers the average value of the hysteresis loops of cycles 5-15 was taken. The shear storage modulus, G', and either the shear loss modulus, G'', or the loss factor, n, govern the main characteristics of the dynamic behavior of viscoelastic and elastomeric materials. All the above parameters can be extracted from each of the hysteresis loops as:

$$G' = \frac{\tau(\gamma=\gamma_{max})-\tau(\gamma=\gamma_{min})}{\gamma_{max}-\gamma_{min}} \tag{1}$$

$$n = \frac{1}{2\pi}\frac{ED}{ES} \tag{2}$$

where $\tau(\gamma = \gamma_{max})$ is the shear stress corresponding to the maximum strain γ_{max}, and $\tau(\gamma = \gamma_{min})$ is the shear stress corresponding to the minimum strain γ_{min}. ED and ES are the dissipated energy per cycle of oscillation, and the maximum energy stored respectively. ED can be calculated based

on the area of the hysteresis loop and ES can be calculated as:

$$ES = \frac{1}{2} G' \gamma_{max}^2 \tag{3}$$

The values of both G' and n for each combination of frequency, amplitude and temperature are shown in Table 2. Equivalent viscous damping ratio can be also calculated as:

$$\zeta_{eq} = \frac{1}{4\pi} \frac{E_D}{E_S} = \frac{n}{2} \tag{4}$$

And in terms of a Kelvin solid model, ζ_{eq} can be also calculated as:

$$\zeta_{eq} = \frac{G'\omega}{2G''} \tag{5}$$

The values of both the loss factor and the shear storage modulus are similar to those of rubbery materials used by (Lee 2003), and other researchers (Teramoto et al. 1996; Soong and Dargush 1997).

As was anticipated, strain amplitude had a larger impact on the EDs' behavior than frequency. This can be more clearly demonstrated by comparing the amplitude dependence at a range of frequencies at fixed temperature, in the form of fig.3. This figure proves the above statement that the dominant factor which affects the elastomer's dynamic behavior is the amplitude and not the frequency, especially in the case of the loss factor, which practically remains the same regardless of any change in frequency. It is also noticeable that when the strain amplitude increases above 30% (which is the key point, as will be shown later, for the transition between the viscoelastic and elastomeric phases) the rates of change of both the shear storage modulus and the loss factor reduce significantly. Below 30%, a large decrease, especially in the loss factor case can be observed. Furthermore, it seems that amplitude and frequency have exactly opposite effects, since increasing strain amplitude leads to decreasing the mechanical properties of the elastomer, while increasing the loading frequency leads to increasing them.

An alternative way of visualizing the elastomer's behavior is by plotting the hysteresis loops of the dampers at each shear strain amplitude, keeping the frequency and temperature constant. Hence, observing fig.4 it can be seen that the elastomer exhibits a behavior which can be rationally approximated as viscoelastic for strain amplitudes of 10%-30%, proving that elastomers exhibit viscoelastic behavior under relatively low amplitudes, which is one of the main material characteristics. The more the strain amplitude increases, the more the hysteresis behavior tends to form a more typical elastomeric shape (compare for example fig.4e, which has slightly different characteristics from the conventional viscoelastic shape, with fig.4a). On the other hand, this is not the case when the frequency is altered. In this case, even though the values of the mechanical properties change, the overall shape of the hysteresis loops remain the same.

When considering the elastomer's dependence on strain amplitude, the fact that not only the mechanical characteristics change, but also the fundamental behavior of the material, makes the modeling procedure of the material extremely difficult. But, at the same time it shows that when the material has larger strain amplitudes, and hence behaves more like a typical elastomer, it tends to be more and more independent of the frequency, in contrast with its viscoelastic phase when the strain amplitudes are relatively low.

With regard to the effect of ambient temperature, both the shear storage modulus, and the loss factor decrease with the increase of temperature. This can be schematically observed by plotting the hysteresis curves of the dampers for different temperatures, while keeping the frequency, and the strain amplitude constant. fig.5 shows how the dissipative capacity of the dampers becomes smaller as the ambient temperature increases. However, it can also be seen that the shape of the hysteresis remains unchanged, leading to the conclusion that only strain amplitude leads to different hysteresis shapes, in contrast with frequency and temperature, which affect, more or less, the dampers' characteristics but not their hysteresis shape.

The effect of the temperature on the elastomers' properties can be more clearly seen in fig. 6, where the values of loss factor and shear storage modulus are plotted against frequency for different temperatures, while keeping the strain amplitude constant at 40%. Two different conclusions can be

made through these figures: a) increase of temperature leads to decrease of dampers' effectiveness. However, the rate of this decrease decreases, as the temperature gets higher, b) the dampers' mechanical properties remain almost constant, especially in the case of the loss factor, with any frequency alteration.

Moreover, similar observations with the 20^{o}C case, can be extracted from the experimental data with regard to the rate of decrease of both shear storage modulus and loss factor. For every given temperature, G' and n tend to alter in a similar way when frequency or strain amplitude changes, leading to the estimation that the elastomer behaves similarly in different temperatures. Even though its mechanical characteristics are reduced, at the same time it seems that any alteration in strain amplitude and frequency results in quite similar change in the loss factor, and the shear storage modulus.

PROPOSED HYSTERESIS MODEL

Linear Generalized Maxwell Model

The proposed model for the hysteresis behavior of the EDs is based on the well known Generalized Maxwell Model (GMM). The GMM has been proposed as numerical representation of VE materials (McCrum et al. 1997; Karavasilis et al. 2011) and can be graphically represented in fig. 7 in force-displacements terms. It consists of linear spring, with stiffness k_0, in parallel with N Maxwell (spring-damper) elements. When stress-strain terms are being used instead, the parameters of fig. 7 have to be adjusted as well. In this paper force-displacements terms are used; however stress-strain terms have been used in literature (Lee 2003; Karavasilis et al. 2011) as well.

The most common procedure of determining the parameters of a VE or elastomeric material, when the GMM is used, is to minimize the error between the analytical values of the shear storage and the shear loss modulus, and the corresponding values which are based on characterization experiments. Based on the assumption that the applied strain has sinusoidal form, with a frequency ω, the corresponding shear storage modulus, G' and the shear loss modulus, G'' can be determined

as (Bland 1960):

$$G' = G_0 + \sum_{i=1}^{N} \frac{G_i \omega^2 {\tau_i}^2}{1 + \omega^2 {\tau_i}^2} \tag{6}$$

$$G'' = \sum_{i=1}^{N} \frac{G_i \omega {\tau_i}^2}{1 + \omega^2 {\tau_i}^2} \tag{7}$$

where

$$\tau_i = \frac{c_i}{k_i} \tag{8}$$

is known as the relaxation time.

The above procedure is based on minimizing the error, on frequency domain, between the analytical expressions of shear storage modulus and shear loss factor and their experimental values, for discrete loading frequencies and is valid only for sinusoidal loading. However, in order to be generalized and validated under random loading, as in the case of seismic loading, these values are normally determined based on a frequency range close to the frequency content of earthquakes (usually 0.25-4 Hz), which is also similar with the content of the natural frequencies of many structures.

Other researchers (Torvik and Bagley 1984; Koh and Kelly 1990; Shen and Soong 1995; Lai et al. 1996; Hwang and Wang 1998) who proposed different models than GMM, such as fractional derivatives model, used the same minimization technique in order to obtain the parameters of their models. However, lack of comparison of experimental data with simulation's models in a hysteresis form, (at least using the cyclic tests with the same frequencies and amplitudes under which these models were initially validated) does not allow the reader to have a better understanding about the behavior of the material under random dynamic loading and about the effectiveness of the proposed model. Shen and Soong (1995) in contrast, compared the hysteresis behavior of test and simulation data, where some discrepancies were noticed.

A different approach was used here, where the main focus of the GMM is on extracting the force-displacement relationship in the time domain for any N number of Maxwell elements, and therefore the model can be validated under any random loading, and potentially capture the hysteresis shape of the elastomer. Although, it is very easy to extract this relationship when only one Maxwell element is used, this becomes much more complicated when more elements are being used.

Initially, a force-displacement relation for the general case of N Maxwell elements was developed based on Laplace transformation. The full derivation is shown in Appendix A and only the final result is presented here:

$$F + \sum_{a=1}^{N} \left[\frac{\partial^a F}{\partial t^a} \{ \sum_{m_i \in A_i} \{ \prod_{r \in B} (\frac{c_r}{k_r}) \} \} \right] = \sum_{\beta=1}^{N} \left[\frac{\partial^\beta u}{\partial t^\beta} \{ \sum_{x_c \in Q_c} \{ \prod_{z \in W} (\frac{c_z}{k_z}) \sum_{z \in W} k_z \} \} \right] + \left[F_0 + \sum_{d=1}^{N} \left[\frac{\partial^d F_0}{\partial t^d} \{ \sum_{p_v \in H_v} \{ \prod_{f \in L} (\frac{c_f}{k_f}) \} \} \right] \right] \tag{9}$$

where:

- u, F, and F_0 represent the displacement, total force, and force corresponding to the linear spring k_0
- $i \in \{1,2,...,\alpha\}$, $c \in \{1,2,...,\beta\}$, $v \in \{1,2,...,d\}$
- $A_i \in \{i, i+1, i+2, ..., N-\alpha+i\}$, $Q_c \in \{c, c+1, c+2, ..., N-\beta+c\}$, $H_v \in \{v, v+1, v+2, ..., N-d+v\}$
- $B \in \{m_1, m_2, ..., m_{\alpha-1}, m_\alpha\}$, $W \in \{x_1, x_2, ..., x_{\beta-1}, x_\beta\}$, and $L \in \{p_1, p_2, ..., p_{d-1}, p_d\}$
- $m_i > m_{i-1}$, $x_c > x_{c-1}$, $p_v > p_{v-1}$ for i, c, $v > 1$

The same process is often carried out with stress-strain, instead of force-displacement terms, although here the latter is preferred. This equation, which is actually a combination of force and displacement derivatives, is valid for every displacement input and for every value of N elements, regardless of the frequency, which represents its main advantage over the classical method described earlier.

The advantage of Eq. 9 compared with the traditional form of the GMM described earlier, apart

from the fact that it may be useful in the mathematical and physical fields, is that it can be used for random loading and not only sinusoidal loading, and the force-displacement relationship can now be extracted in the time domain for any number N of Maxwell elements, capturing the material's hysteresis shape, and is not based on minimizing the error between the analytical expressions of the shear storage modulus and their corresponding experimental values. Furthermore, it can be also concluded that Eq.9 is very similar with the force-displacement relationship of the Generalized Derivatives model (Nashif et al. 1985), which has also been used for modeling elastomeric behavior (Torvik and Bagley 1984; Koh and Kelly 1990; Hwang and Wang 1998). However, the unknown parameters of the Generalized Derivatives equation are now determined, and are functions of the stiffness k_i, and the damping coefficients c_i of the GMM. Replacing the integral derivatives with fractional derivatives, the generalised model is changed to the well known fractional derivative model (Nashif et al. 1985). Another restriction of either Generalized Derivatives or Fractional Derivatives model is the way they have been implemented in order to extract their parameters; the same minimization technique which was mentioned earlier for the GMM is used here as well (Nashif et al. 1985). Furthermore, even though Fractional Derivative models are usually based on fewer parameters, it was found that additional parameters were necessary to capture the dynamic characteristics of the EDs tested.

When more simplifying procedures are preferred, especially for design purposes or preliminary analysis of structures, a simplified Kelvin-Voigt model (spring and dashpot connected in parallel) can be used, the parameters of which can be determined based on the natural frequency of the structure and a design permitted damper displacement.

Modified Generalized Maxwell Model

In trying to fit the GMM to the experimental data, it was found that the GMM was only adequate to describe VE behavior, regardless of the number of Maxwell elements used, and could not adequately represent the frequency or amplitude dependence. Hence, a Modified Generalized

Maxwell Model (MGMM) is proposed here. In order to take into account the non linear part of the elastomer's behavior, a non linear damper was added to the main GMM equation:

$$F_{NL} = c_{NL}|\dot{u}|^{\alpha} sgn(\dot{u}) \tag{10}$$

It was also found that the ED's behavior depended on both the maximum displacement and the maximum velocity obtained during the loading history. Karavasilis et al. (2012) proposed a modified stiffness based on the maximum displacement to take into account the softening of the elastomer:

$$k_{mod} = k_a e^{-\frac{u_{max}}{u_{ref}}} + k_b \tag{11}$$

where k_{a}, k_{b} and u_{ref} are constants, and u_{max} is the average of the maximum absolute deformation amplitudes in the negative ($u_{\mathrm{max,n}}$) and positive ($u_{\mathrm{max,p}}$) directions, and can be determined as follows:

$$u_{max} = \frac{u_{max,p} + |u_{max,n}|}{2} \tag{12}$$

The values of $u_{\mathrm{max,p}}$ and $u_{\mathrm{max,n}}$ are updated at every time step and are fed into the constitutive equation to calculate the overall response. Similar modeling approach was followed by Summers (2004). Following the same philosophy in terms of velocity instead of displacement, a modified damping coefficient is introduced here, which was found to significantly contribute to the elastomer's dynamic behavior:

$$c_{mod} = c_a e^{-\frac{v_{max}}{v_{ref}}} + c_b \tag{13}$$

The parameters c_{a}, c_{b}, v_{ref}, and v_{max} are defined in a similar way to the terms in k_{mod}, of Eq. 11.

Hence, the final form of the Modified Generalized Maxwell Model (MGMM) consists of the

following parts:

- The linear GMM obtained from Equation 9
- The final version of F_0, which consists of a linear spring:

$$F_0 = k_0 u \tag{14}$$

- The non linear damper, Eq. 10
- The modified stiffness, Eq. 11
- The modified damping coefficient, Eq. 13

Since a generalized equation for N Maxwell elements was now available, efforts were made to use more than one element. Analytical models were determined with $N = 2, 3$ and 4 Maxwell elements. However, it was found that using only one Maxwell element was adequate for the specific material without significant compromise in accuracy. Hence, using $N = 1$, Eq. 9 simplifies to:

$$F + \frac{c_1}{k_1}\dot{F} = F_0 + \frac{c_1}{k_1}\dot{F}_0 + c_1\dot{u} \tag{15}$$

where $\dot{F}$ and $\dot{u}$ denote the differentiation of the force and the displacement with respect to time.

Therefore, incorporating the additional non-linear terms, the final constitutive equation for the dynamic behavior of the elastomeric dampers is:

$$F + \frac{c_1}{k_1}\dot{F} = (k_0 + k_{mod})u + (\frac{c_1}{k_1}k_0 + c_1 + c_{mod})\dot{u} + c_{NL}|\dot{u}|^{\alpha} sgn(\dot{u}) \tag{16}$$

Parameter Estimation

Least square minimization is one of the most widely used methods (Fan; Lee; Karavasilis et al.) of fitting the numerical parameters of a proposed model into the experimental data. However, as mentioned earlier, in case of the GMM this minimization technique has been based on the frequency domain, trying to minimize the shear storage modulus (from Eq.6), and the loss factor, $n = \frac{G''}{G'}$ (combining Eq.6, and Eq.7) for every frequency and temperature that the damper was experimentally tested, as:

$$min\Big\{\sum_{j=1}^{N}\Big[G'_{anal} - G'_{exp}\Big]^2\Big\} \tag{17}$$

$$min\Big\{\sum_{j=1}^{N}\Big[n_{anal} - n_{exp}\Big]^2\Big\} \tag{18}$$

where N denotes the number of experimental data available. With regard to fitting the numerical model to the experimental data, researchers have used various techniques. The most common is to assume constant one of the three main parameters that the material is dependent upon (strain amplitude, loading frequency, ambient temperature) (Fan 1998). On the other hand, minimization of the corresponding error for every cyclic test has been used as well (Karavasilis et al. 2012), taking the average value of these parameters in order to generate the model through the whole range of shear strain amplitudes, frequencies, and temperatures. Finally, another widely used method is to include all the available data into one least square equation (Lee 2003).

In the case of models which were minimized based on their shear storage modulus, and loss factor for specific frequencies, even though the numerical values of G' and n seem to fit well with the experimental data, the corresponding model will not necessarily be valid in the time domain for random loading (and more specifically for random displacements), since these parameters will only be adequate to predict the shear storage modulus, and the loss factor of the damper under cyclic testing with constant frequency, and constant maximum displacement, and not the actual

elastomer's dynamic behavior.

Another approach was therefore used here, which takes into account the variability of displacements. Sweep amplitude sinusoidal tests (with the shear strain amplitude ranging from 10%-50%), which were carried out for the same frequency range used in the characterization tests, formed the basis for the minimization. The sweep amplitude tests were based on proposals from Dorka and Garcia (2005). Keeping the frequency and the temperature constant within each test, and setting the maximum strain amplitude to be 50%, the sweep amplitude tests consisted of the following steps: 1.5 cycles of $u_{max}/2$, 1.5 cycles of u_{max}, 1.5 cycles of $u_{max}/3$, 1.5 cycles of $u_{max}/6$, 1.5 cycles of $u_{max}/2$, 1.5 cycles of $2u_{max}/3$, 1.5 cycles of $5u_{max}/6$, 3 cycles of u_{max}, 1.5 cycles of $5u_{max}/6$, 1.5 cycles of $2u_{max}/3$, 1.5 cycles of $u_{max}/2$, 1.5 cycles of $u_{max}/3$, 1.5 cycles of $u_{max}/6$. Fig. 8 shows a typical example of both the sweep sinusoidal command displacement and the ED's response for a test at a frequency of 3.0 Hz.

The sweep amplitude test is believed to be a more representative test compared with tests based on fixed strain amplitude and frequency, at least for fitting the parameters because of the strong amplitude dependence of the elastomer. The MGMM (Eq. 16) contains 11 parameters which need to be determined: k_1, c_1, k_0, k_a, k_b, u_ref, c_a, c_b, v_ref, c_NL, α. In order to optimize these parameters a least square method was used:

$$min\Big\{\sum_i \sum_k \Big[F_{anal(i,k)} - F_{exp(i,k)}\Big]^2\Big\} \tag{19}$$

where i is the index for frequency content (e.g., $i = 2$ is equivalent with frequency of 0.5 Hz), and k stands for the force-displacement data set at a specific frequency and displacement. In order to separate strain rate dependent and independent components of the model, stress relaxation tests along with very low frequency (0.01 Hz) cyclic tests in a range of strain amplitudes were carried out. These experiments allowed the separation of the strain rate dependent and independent parts of the stress. And therefore, quantifying the strain rate dependent damper's behaviour could be achieved due to these tests.

Table 3 provides the parameters of the hysteresis model, while Fig. 9 shows the hysteresis response of the damper for both the analytical and experimental case. It can be seen that the results are in a very good agreement. It is also worth mentioning that the proposed model is valid under any random loading, and its parameters do not depend on the imposed displacement or frequency.

In order to evaluate the effectiveness of GMM as well, experimental data of 0.5 and 2.0 Hz were compared with a GMM. Parameters of the GMM were obtained following the exact same process which was followed with MGMM. Fig. 10 shows this comparison, where the NRMS error for the data of 0.5 and 2.0 Hz is 8.1% and 2.43% respectively. Two things worth mentioning based on the GMM model. First, that even though GMM can acceptably capture the behavior of the material when the frequency of the loading remains constant, this is not the case when the frequency changes, even slightly. Second, as it can be seen from these figures, comparing simulation and experimental results in Force-Time relationship may be misleading, as it was mentioned earlier as well. Figs. 10a, and 10b show that what seems like a good agreement in Force-Time relationship, is not really acceptable as a solution when it is compared in Force-Displacement terms.

Effect of Temperature

In order to capture the behavior of the EDs under different ambient temperatures, both the characterization tests and the sweep amplitude tests were repeated at different temperatures: 25, 30, and 35^{o}C. The same model (MGMM), which was developed and validated for the experiments which were carried out at room temperature (20^{o}C), will be used here as well, by introducing a new parameter, γ_T. A simplifying assumption that all parameters change at the same rate with temperature was made. This assumption was considered as a simplifying tool when optimizing the parameters of the model under different temperatures, and can be seen as an additional empirical value. This led to a much more adjustable model, according to which the only parameter that needs to be specified when different ambient temperatures are applied, is the proposed parameter, γ_T. Alternatively, additional optimization techniques identical with the ones carried out for room temperature, have to be used in the 25-35^{o}C range in order to re-optimize the parameters of the model under the new temperatures. This alternative solution was also carried out and it was found

out that the values of the new parameters were almost the same as the original ones multiplied by γ_T. Hence, the first approach was adapted here. The comparison of experimental and simulation data led to a very good agreement. The original proposed hysteresis model in this case has been adjusted:

$$F_T + \frac{c_1}{k_1}\dot{F}_T = (\gamma_T k_0 + k_{mod,T})u + (\frac{c_1}{k_1}k_0\gamma_T + \gamma_T c_1 + c_{mod,T})\dot{u} + \gamma_T k_{NL}(\dot{u})^{\alpha\gamma_T} \tag{20}$$

where:

$$c_{mod,T} = \gamma_T c_a e^{-\frac{v_{max}}{\gamma_T v_{ref}}} + \gamma_T c_b \tag{21}$$

and

$$k_{mod,T} = \gamma_T k_a e^{-\frac{u_{max}}{\gamma_T u_{ref}}} + \gamma_T k_b \tag{22}$$

where T denotes the ambient temperature, and γ_T the coefficient which controls the parameters of the model in different temperatures. Again, the same minimization techniques introduced earlier were used to determine the γ_T parameter for different temperatures. These values are summarized in Table 4.

As expected from the results of the characterization tests carried out at different temperatures, the values of γ_T reduce with the increase of temperature. This reduction can be schematically seen at Fig. 11 and can be approximately determined as 0.116/^{o}C. A more quantified approach is given in Table 5 where the Normalized Root Mean Square (NRMS) error has been calculated for every sweep amplitude test which was carried out under the aforementioned ranges of frequencies and temperatures. It can be seen that the the proposed constitutive model can accurately predict the response of the elastomer under any frequency, strain amplitude or ambient temperature, since the maximum NRMS error observed during these tests was 1.83%.

It should be noted that this model takes into account the ambient temperature during the test, and not the temperature due to energy dissipation of the damper. Due to the limited number of cycles used in this study, the temperature rise during the tests was not found to be dominant factor to the proposed model. However, if the material is tested under more cycles, for validation against wind loading for example, then this alteration of temperature should be taken into account.

Moreover, in order to evaluate the efficiency of the proposed model, in terms of dissipative energy, Figs 12 and 13 can be used which compare the energy dissipation extracted from the model with the dissipation energy obtained from the characterization tests, for T=20C and T= 30C, for every strain amplitude and frequency. It can be seen that dissipation energy is another parameter which shows the efficiency of the proposed model.

CONCLUSIONS

A constitutive equation, which is able to capture the dynamic characteristics of an elastomeric damper, is proposed in this study. The properties of the damper were first measured experimentally over a wide range of frequencies, amplitudes and temperatures. It was seen that strain amplitude had the largest impact on the EDs behavior. It was also concluded that the loss factor of the material is almost constant when frequency changes. The most noticeable remark though, is the change of elastomer's behavior, which can be only captured by comparing hysteresis behavior, when the strain amplitude increases above 30%. Therefore, not only the mechanical parameters of the material change, but also the hysteresis shape itself. It was shown that when the material has larger strain amplitudes it behaves more like a typical elastomer, and tends to be more and more independent of the frequency, in contrast with its viscoelastic phase when the strain amplitudes are relatively low.

In order to capture this behavior a new constitutive model was presented, based on a modified version of GMM. It was found that, for our system, a GMM with a single spring-damper (N = 1) was sufficient, with the addition of further elements giving only modest improvements in performance. However, it was then necessary to modify this linear model through the addition of amplitude-related adjustments to stiffness and damping terms, and a further non-linear damping term. The model was then extended to include a simple adjustment to account for variations in ambient temperature. The

material parameters of this model have been identified using experimental results. The resulting model, termed the Modified GMM, shows excellent agreement with the experimental results across a wide range of operating conditions.

DATA AVAILABILITY STATEMENT

All data, models, and code generated or used during the study appear in the submitted article.

ACKNOWLEDGEMENTS

We thank Alan Muhr and Hamid Ahmadi of the Tun Abdul Razak Research Centre for their support of this work and the donation of test devices, and the UK Engineering and Physical Sciences Research Council for their financial support of the first author.

APPENDIX I. FORCE-DISPLACEMENT RELATIONSHIP OF GENERALIZED MAXWELL MODEL

As already mentioned the Generalized Maxwell Model (GMM) is a series of Maxwell elements assembled in parallel along with a linear spring (Fig. 7). For every Maxwell element the force displacement relationship in time domain is given as:

$$k_i F_i + c_i \frac{dF_i}{dt} = k_i c_i \frac{du_i}{dt} \tag{23}$$

where k_i and c_i are the stiffness and the dashpot coefficients of the ith Maxwell element, u_i is the imposed displacement and F_i the corresponding force. In the case of parallel connection of Maxwell elements $u_i = u$ for every, i, Maxwell element. Assuming zero initial conditions for both the displacement and the force, and applying Laplace Transformation to Eq.23:

$$(k_i + c_i s) F_{i,L} = k_i c_i s u_L \tag{24}$$

where $F_\mathrm{i,L}$ is the Laplace transform of the force corresponding to the i Maxwell element, and u_L is the Laplace transform of the displacement. Equation 24 can be rewritten in the following form:

$$F_{i,L} = \frac{k_i c_i s}{k_i + c_i s} u_L \tag{25}$$

And for N Maxwell elements the Laplace transform of the total force can be determined as:

$$F_L = \sum_{i=1}^{N} F_{i,L} + F_{0,L} = \sum_{i=1}^{N} \frac{k_i c_i s}{k_i + c_i s} u_L + F_{0,L} \tag{26}$$

where $F_{0,L}$ represents the Laplace transform of the additional force corresponding to the linear spring (in this case), which is connected in parallel with the N Maxwell elements. Multiplying throughout by the minimum common multiple of the denominators of the operators of the right

side of Equation 26 and rearranging:

$$\Big[\prod_{h=1}^{N}(k_h + c_h s)\Big]F_L = \sum_{i=1}^{N}\Big[(k_i c_i s)\prod_{j=1}^{N}(k_j + c_j s)\Big]u_L + \Big[\prod_{g=1}^{N}(k_g + c_g s)\Big]F_{0,L} \tag{27}$$

where $j \neq i$, Σ represents summation, and Π represents a series multiplication

Focusing only on the left part of the Equation 27:

$$\begin{gathered}
\Big[\prod_{h=1}^{N}(k_h + c_h s)\Big]F_L = \\
\Big[(k_1 + c_1 s)(k_2 + c_2 s)(k_3 + c_3 s)...(k_{N-1} + c_{N-1} s)(k_N + c_N s)\Big]F_L = \\
\Big[(k_1 k_2 k_3 ... k_{N-2} k_{N-1} k_N) + \\
(k_1 k_2 k_3 ... k_{N-2} k_{N-1} c_N + k_1 k_2 k_3 ... k_{N-2} k_N c_{N-1} + ... + \\
k_1 k_3 ... k_{N-2} k_{N-1} k_N c_2 + k_2 k_3 ... k_{N-2} k_{N-1} k_N c_1) s + \\
(k_1 k_2 k_3 ... k_{N-2} c_{N-1} c_N + k_1 k_2 k_3 ... k_{N-4} k_{N-3} k_{N-1} c_{N-2} c_N + ... + \\
k_1 k_4 k_5 ... k_{N-2} k_{N-1} k_N c_2 c_3 + k_3 k_4 k_5 ... k_{N-2} k_{N-1} k_N c_1 c_2) s^2 + \\
(k_1 k_2 k_3 ... k_{N-4} k_{N-3} c_{N-2} c_{N-1} c_N + k_1 k_2 k_3 ... k_{N-4} k_{N-2} c_{N-3} c_{N-1} c_N + ... + \\
k_1 k_5 k_6 ... k_{N-1} k_N c_2 c_3 c_4 + k_4 k_5 k_6 ... k_{N-1} k_N c_1 c_2 c_3) s^3 \\
+ ... + \\
(k_1 c_2 c_3 ... c_{N-2} c_{N-1} c_N + k_2 c_1 c_3 ... c_{N-2} c_{N-1} c_N + ... + \\
k_{N-1} c_1 c_2 ... c_{N-3} c_{N-2} c_N + k_N c_1 c_2 ... c_{N-2} c_{N-1}) s^{N-1} + \\
(c_1 c_2 c_3 ... c_{N-2} c_{N-1} c_N) s^N \Big] F_L
\end{gathered} \tag{28}$$

Dividing Equation 28 by $\prod_{d=1}^{N}(k_d)$:

$$\begin{gathered}\Big[1+(\tfrac{c_N}{k_N}+\tfrac{c_{N-1}}{k_{N-1}}+\ldots+\tfrac{c_2}{k_2}+\tfrac{c_1}{k_1})s+\\ (\tfrac{c_N}{k_N}\tfrac{c_{N-1}}{k_{N-1}}+\tfrac{c_N}{k_N}\tfrac{c_{N-2}}{k_{N-2}}+\tfrac{c_N}{k_N}\tfrac{c_{N-3}}{k_{N-3}}+\ldots+\tfrac{c_2}{k_2}\tfrac{c_3}{k_3}+\tfrac{c_1}{k_1}\tfrac{c_2}{k_2})s^2+\\ (\tfrac{c_N}{k_N}\tfrac{c_{N-1}}{k_{N-1}}\tfrac{c_{N-2}}{k_{N-2}}+\tfrac{c_N}{k_N}\tfrac{c_{N-1}}{k_{N-1}}\tfrac{c_{N-3}}{k_{N-3}}+\ldots+\tfrac{c_2}{k_2}\tfrac{c_3}{k_3}\tfrac{c_4}{k_4}+\tfrac{c_1}{k_1}\tfrac{c_2}{k_2}\tfrac{c_3}{k_3})s^3\\ +\ldots+\\ (\tfrac{c_2}{k_2}\tfrac{c_3}{k_3}\cdots\tfrac{c_{N-1}}{k_{N-1}}\tfrac{c_N}{k_N}+\tfrac{c_1}{k_1}\tfrac{c_3}{k_3}\cdots\tfrac{c_{N-1}}{k_{N-1}}\tfrac{c_N}{k_N}+\ldots+\tfrac{c_1}{k_1}\tfrac{c_2}{k_2}\cdots\tfrac{c_{N-3}}{k_{N-3}}\tfrac{c_{N-2}}{k_{N-2}}\tfrac{c_N}{k_N}+\tfrac{c_1}{k_1}\tfrac{c_2}{k_2}\cdots\tfrac{c_{N-2}}{k_{N-2}}\tfrac{c_{N-1}}{k_{N-1}})s^{N-1}+\\ (\tfrac{c_1}{k_1}\tfrac{c_2}{k_2}\cdots\tfrac{c_{N-1}}{k_{N-1}}\tfrac{c_N}{k_N})s^N\Big]F_L\end{gathered} \tag{29}$$

Equation 29 can be rewritten in the following format:

$$F_L+\sum_{a=1}^{N}\Big[s^a F_L\{\sum_{m_i\in A_i}\{\prod_{r\in B}(\frac{c_r}{k_r})\}\}\Big] \tag{30}$$

where:

- $i\in\{1,2,...,\alpha\}$
- $A_i\in\{i,i+1,i+2,...,N-\alpha+i\}$
- $m_i>m_{i-1}$, for $i>1$
- $B\in\{m_1,m_2,...,m_{\alpha-1},m_\alpha\}$

Focusing now on the first part of the right hand side of Equation 27:

$$\begin{gathered}\Big[\sum_{i=1}^{N}(k_i c_i s)\prod_{j=1}^{N}(k_j+c_j s)\Big]u_L=\\ \Big[k_1c_1s(k_2+c_2s)(k_3+c_3s)\ldots(k_{N-1}+c_{N-1}s)(k_N+c_Ns)+\\ k_2c_2s(k_1+c_1s)(k_3+c_3s)\ldots(k_{N-1}+c_{N-1}s)(k_N+c_Ns)+\\ +\ldots+\\ k_{N-1}c_{N-1}s(k_1+c_1s)(k_2+c_2s)\ldots(k_{N-2}+c_{N-2}s)(k_N+c_Ns)+\\ k_Nc_Ns(k_1+c_1s)(k_2+c_2s)\ldots(k_{N-2}+c_{N-2}s)(k_{N-1}+c_{N-1}s)\Big]u_L\end{gathered} \tag{31}$$

Equation31 can be rewritten as:

$$\begin{gathered}\Bigg[\Big[(c_1+c_2+\ldots+c_{N-1}+c_N)k_1k_2\ldots k_{N-1}k_N\Big]s+\\ \Big[c_1c_2(k_1+k_2)k_3\ldots k_N+c_1c_3(k_1+k_3)k_2k_4\ldots k_N+\ldots+\\ c_{N-1}c_N(k_{N-1}+k_N)k_1k_2\ldots k_{N-2}\Big]s^2+\\ \Big[c_1c_2c_3(k_1+k_2+k_3)k_4\ldots k_N+c_1c_2c_4(k_1+k_2+k_4)k_3k_5\ldots k_N+\ldots+\\ c_{N-2}c_{N-1}c_N(k_{N-2}+k_{N-1}+k_N)k_1\ldots k_{N-3}\Big]s^3\\ +\ldots+\\ \Big[c_1c_2\ldots c_{N-2}c_{N-1}(k_1+k_2+\ldots+k_{N-2}+k_{N-1})k_N+\ldots+\\ c_2c_3\ldots c_{N-1}c_N(k_2+k_3\ldots+k_{N-1}+k_N)k_1\Big]s^{N-1}+\\ \Big[c_1c_2\ldots c_{N-1}c_N(k_1+k_2+\ldots+k_{N-1}+k_N)\Big]s^N\Bigg]u_L\end{gathered} \tag{32}$$

And now dividing Equation 32 by $\prod_{d=1}^{N}(k_d)$, as was done with Equation28:

$$\begin{gathered}\Bigg[\Big[c_1+c_2+\ldots+c_{N-1}+c_N\Big]s+\\ \Big[\tfrac{c_1}{k_1}\tfrac{c_2}{k_2}(k_1+k_2)+\tfrac{c_1}{k_1}\tfrac{c_3}{k_3}(k_1+k_3)+\ldots+\\ \tfrac{c_{N-2}}{k_{N-2}}\tfrac{c_{N-1}}{k_{N-1}}(k_{N-2}+k_{N-1})+\tfrac{c_{N-1}}{k_{N-1}}\tfrac{c_N}{k_N}(k_{N-1}+k_N)\Big]s^2+\\ \Big[\tfrac{c_1}{k_1}\tfrac{c_2}{k_2}\tfrac{c_3}{k_3}(k_1+k_2+k_3)+\tfrac{c_1}{k_1}\tfrac{c_2}{k_2}\tfrac{c_4}{k_4}(k_1+k_2+k_4)+\ldots+\\ \tfrac{c_{N-2}}{k_{N-2}}\tfrac{c_{N-1}}{k_{N-1}}\tfrac{c_N}{k_N}(k_{N-2}+k_{N-1}+k_N)\Big]s^3\\ +\ldots+\\ \Big[\tfrac{c_1}{k_1}\tfrac{c_2}{k_2}\ldots\tfrac{c_{N-2}}{k_{N-2}}\tfrac{c_{N-1}}{k_{N-1}}(k_1+k_2+\ldots+k_{N-2}+k_{N-1})+\\ \tfrac{c_1}{k_1}\tfrac{c_3}{k_3}\ldots\tfrac{c_{N-1}}{k_{N-1}}\tfrac{c_N}{k_N}(k_1+k_3+\ldots+k_{N-1}+k_N)+\ldots+\\ \tfrac{c_2}{k_2}\tfrac{c_3}{k_3}\ldots\tfrac{c_{N-1}}{k_{N-1}}\tfrac{c_N}{k_N}(k_2+k_3+\ldots+k_{N-1}+k_N)\Big]s^{N-1}+\\ \Big[\tfrac{c_1}{k_1}\tfrac{c_2}{k_2}\ldots\tfrac{c_{N-1}}{k_{N-1}}\tfrac{c_N}{k_N}(k_1+k_2+\ldots+k_{N-1}+k_N)\Big]s^N\Bigg]u_L\end{gathered} \tag{33}$$

Which leads to:

$$\sum_{\beta=1}^{N}\left[s^{\beta}u_{L}\{\sum_{x_{c}\in Q_{c}}\{\prod_{z\in W}(\frac{c_{z}}{k_{z}})\sum_{z\in W}k_{z}\}\}\right] \tag{34}$$

where:

- c∈{1,2,...,β}
- Q_c∈{c,c+1,c+2,...,N-β+c}
- x_c>$x_{c\text{-}1}$ for c>1
- W∈{x_1,x_2,...,$x_{\beta\text{-}1}$,x_β}

The last part of the right hand side of the Equation 27 can be similarly rearranged with its left part and can be presented in its final format:

$$F_{0,L}+\sum_{d=1}^{N}\left[s^{d}F_{0,L}\{\sum_{p_{v}\in H_{v}}\{\prod_{f\in L}(\frac{c_{f}}{k_{f}})\}\}\right] \tag{35}$$

where:

- v∈{1,2,...,d}
- H_v∈{v,v+1,v+2,...,N-d+v}
- p_v>$p_{v\text{-}1}$ for v>1
- L∈{p_1,p_2,...,$p_{d\text{-}1}$,p_d}

Combining Equations 30,34, and 35, then 27 can be rewritten as:

$$\begin{gathered}F_{L}+\sum_{a=1}^{N}\left[s^{a}F_{L}\{\sum_{m_{i}\in A_{i}}\{\prod_{r\in B}(\frac{c_{r}}{k_{r}})\}\}\right]\ =\\ \sum_{\beta=1}^{N}\left[s^{\beta}u_{L}\{\sum_{x_{c}\in Q_{c}}\{\prod_{z\in W}(\frac{c_{z}}{k_{z}})\sum_{z\in W}k_{z}\}\}\right]+\left[F_{0,L}+\sum_{d=1}^{N}\left[s^{d}F_{0,L}\{\sum_{p_{v}\in H_{v}}\{\prod_{f\in L}(\frac{c_{f}}{k_{f}})\}\}\right]\right]\end{gathered} \tag{36}$$

Finally, applying inverse Laplace transformation to 36:

$$F+\sum_{a=1}^{N}\left[\frac{\partial^a F}{\partial t^a}\{\sum_{m_i\in A_i}\{\prod_{r\in B}(\frac{c_r}{k_r})\}\}\right]=$$
$$\sum_{\beta=1}^{N}\left[\frac{\partial^\beta u}{\partial t^\beta}\{\sum_{x_c\in Q_c}\{\prod_{z\in W}(\frac{c_z}{k_z})\sum_{z\in W}k_z\}\}\right]+\left[F_0+\sum_{d=1}^{N}\left[\frac{\partial^d F_0}{\partial t^d}\{\sum_{p_v\in H_v}\{\prod_{f\in L}(\frac{c_f}{k_f})\}\}\right]\right] \tag{37}$$

where:

- $i\in\{1,2,...,\alpha\}$, c$\in\{1,2,...,\beta\}$, $v\in\{1,2,...,$d$\}$
- $A_i\in\{i,i+1,i+2,...,N-\alpha+i\}$, $Q_c\in\{c,c+1,c+2,...,N-\beta+c\}$, $H_v\in\{v,v+1,v+2,...,N-d+v\}$
- B$\in\{m_1,m_2,...,m_{\alpha-1},m_\alpha\}$, W$\in\{x_1,x_2,...,x_{\beta-1},x_\beta\}$, and L$\in\{p_1,p_2,...,p_{d-1},p_d\}$
- $m_i>m_{i-1}$, $x_c>x_{c-1}$, $p_v>p_{v-1}$ for i, c, $v>1$

For illustrative purposes, the cases of N=1, N=2, and N=3 will be presented. If N=1 Eq. 37 becomes:

$$F+\frac{dF}{dt}[\frac{c_1}{k_1}]=F_0+\frac{dF_0}{dt}\frac{c_1}{k_1}+\frac{du}{dt}c_1 \tag{38}$$

In the case of N=2 Eq. 37 is determined as:

$$F+\frac{dF}{dt}[\frac{c_1}{k_1}+\frac{c_2}{k_2}]+\frac{d^2F}{dt^2}[\frac{c_1}{k_1}\frac{c_2}{k_2}]=F_0+\frac{dF_0}{dt}[\frac{c_1}{k_1}+\frac{c_2}{k_2}]+\frac{d^2F_0}{dt^2}[\frac{c_1}{k_1}\frac{c_2}{k_2}]+$$
$$\frac{du}{dt}[c_1+c_2]+\frac{d^2u}{dt^2}[\frac{c_1}{k_1}\frac{c_2}{k_2}(k_1+k_2)] \tag{39}$$

In the case of N=3 Eq. 37 is determined as:

$$F+\frac{dF}{dt}[\frac{c_1}{k_1}+\frac{c_2}{k_2}+\frac{c_3}{k_3}]+\frac{d^2F}{dt^2}[\frac{c_1}{k_1}\frac{c_2}{k_2}+\frac{c_1}{k_1}\frac{c_3}{k_3}+\frac{c_2}{k_2}\frac{c_3}{k_3}]+\frac{d^3F}{dt^3}[\frac{c_1}{k_1}\frac{c_2}{k_2}\frac{c_3}{k_3}]=$$
$$F_0+\frac{dF_0}{dt}[\frac{c_1}{k_1}+\frac{c_2}{k_2}+\frac{c_3}{k_3}]+\frac{d^2F_0}{dt^2}[\frac{c_1}{k_1}\frac{c_2}{k_2}+\frac{c_1}{k_1}\frac{c_3}{k_3}+\frac{c_2}{k_2}\frac{c_3}{k_3}]+\frac{d^3F_0}{dt^3}[\frac{c_1}{k_1}\frac{c_2}{k_2}\frac{c_3}{k_3}]+$$
$$\frac{du}{dt}[c_1+c_2+c_3]+\frac{d^2u}{dt^2}[\frac{c_1}{k_1}\frac{c_2}{k_2}(k_1+k_2)+\frac{c_1}{k_1}\frac{c_3}{k_3}(k_1+k_3)+\frac{c_2}{k_2}\frac{c_3}{k_3}(k_2+k_3)]+$$
$$\frac{d^3u}{dt^3}[\frac{c_1}{k_1}\frac{c_2}{k_2}\frac{c_3}{k_3}(k_1+k_2+k_3)] \tag{40}$$

REFERENCES

Aiken, I. (1997). "An analytical hysteresis model for elastomeric seismic isolation bearings." *Earthquake Engineering and Structural Dynamics*, 26(2).

Bland, D. (1960). *The Theory of Linear Viscoelasticity, Pergamon Press, Oxford, 1960*.

Constantinou, M. C., Soong, T. T., and Dargush, G. F. (1998). *Passive energy dissipation systems for structural design and retrofit*. Multidisciplinary Center for Earthquake Engineering Research Buffalo, New York.

Constantinou, M. C. and Tadjbakhsh, I. G. (1985). "Hysteretic dampers in base isolation: random approach." *Journal of Structural Engineering*, 111(4), 705–721.

Dahl, P. R. (1968). *A solid friction model*. Aerospace Corp El Segundo Ca.

Dorka, U. and Garcia, J. (2005). "Seismic qualification of passive mitigation devices." *Report no.1,2005*, Cooperative Advancements in Seismic and Dynamic Experiments (CASCADE).

Fan, C. P. (1998). *Seismic Analysis, Behavior, and Retrofit of Non-Ductile Reinforced Concrete Frame Buildings with Viscoelastic Dampers*. Ph.D. Dissertation, Department of Civil and Environmental Engineering, Lehigh University.

Ferry, J. D. (1980). *Viscoelastic properties of polymers*. John Wiley & Sons.

Hepburn, C. and Reynolds, R. (1979). *Elastomers: Criteria for Engineering Design*. Applied Science Publishers, London.

Hwang, J. and Wang, J. (1998). "Seismic response prediction of hdr bearings using fractional derivative maxwell model." *Engineering Structures*, 20(9), 849–856.

Jrad, H., Dion, J. L., Renaud, F., Tawfiq, I., and Haddar, M. (2013). "Experimental characterization, modeling and parametric identification of the non linear dynamic behavior of viscoelastic components." *European Journal of Mechanics - A/Solids*, 42, 176 – 187.

Jrad, H., Dion, J. L., Renaud, F., Tawfiq, I., and Haddar, M. (2017). "Experimental and numerical investigation of energy dissipation in elastomeric rotational joint under harmonic loading." *Mechanics of Time-Dependent Materials*, 21(2), 177–198.

Karavasilis, T. L., Blakeborough, T., and Williams, M. S. (2011). "Development of nonlinear

analytical model and seismic analyses of a steel frame with self-centering devices and viscoelastic dampers." *Computers & Structures*, 89(11), 1232–1240.

Karavasilis, T. L., Sause, R., and Ricles, J. M. (2012). "Seismic design and evaluation of steel moment-resisting frames with compressed elastomer dampers." *Earthquake Engineering & Structural Dynamics*, 41(3), 411–429.

Kit Miyamoto, M. and Lon M. Determan, S. "Structural Applications of Taylor Fluid Viscous Dampers, <http://www.taylordevices.com/custom/pdf/tech-papers/70-SeismicRehabilitationofHCS.pdf>.

Koh, C. G. and Kelly, J. M. (1990). "Application of fractional derivatives to seismic analysis of base-isolated models." *Earthquake engineering & structural dynamics*, 19(2), 229–241.

Kästner, M., Obst, M., Brummund, J., Thielsch, K., and Ulbricht, V. (2012). "Inelastic material behavior of polymers – experimental characterization, formulation and implementation of a material model." *Mechanics of Materials*, 52, 40 – 57.

Lai, M., Lu, P., Lunsford, D., Kasai, K., and Chang, K. (1996). "Viscoelastic damper: a damper with linear or nonlinear material." *Proceedings of 11th World Conference on Earthquake Engineering*.

Lee, K. S. (2003). *Seismic Behavior of Structures with Dampers Made from Ultra High Damping Natural Rubber*. Ph.D. Dissertation, Department of Civil and Environmental Engineering, Lehigh University.

Mahmoodi, P., Robertson, L., Yontar, M., Moy, C., and Feld, L. (1987). "Performance of viscoelastic dampers in world trade center towers." *Dynamics of structures*, ASCE, 632–644.

Makris, N. and Constantinou, M. (1991). "Fractional-derivative maxwell model for viscous dampers." *Journal of Structural Engineering*, 117(9), 2708–2724.

McCrum, N. G., Buckley, C., and Bucknall, C. B. (1997). *Principles of polymer engineering*. Oxford University Press, USA.

Muhr, A. (22 October 2019). *Personal Communication with TARRC*.

Nashif, A. D., Jones, D. I., and Henderson, J. P. (1985). *Vibration damping*. John Wiley & Sons.

Pant, D., Montgomery, M., Christopoulos, C., and Poon, D. (2017). "Viscoelastic coupling dampers

for the enhanced seismic resilience of a megatall building." *16th World Conference on Earthquake Engineering, 16WCEE 2017*, Vol. 1318.

Papoulia, K. D. and Kelly, J. M. (1994). *Material characterization of elastomers used in earthquake base isolation*. Earthquake Engineering Research Center, University of California.

Petrone, F., Lacagnina, M., and Scionti, M. (2004). "Dynamic characterization of elastomers and identification with rheological models." *Journal of Sound and Vibration*, 271(1), 339 – 363.

Prestandard (2000). "commentary for the seismic rehabilitation of buildings (fema356)." *Washington, DC: Federal Emergency Management Agency*, 7.

Sause, R., Lee, K.-S., and Ricles, J. (2007). "Rate-independent and rate-dependent models for hysteretic behavior of elastomers." *Journal of Engineering Mechanics*, 133(11), 1162–1170.

Shen, K. and Soong, T. (1995). "Modeling of viscoelastic dampers for structural applications." *Journal of Engineering Mechanics*, 121(6), 694–701.

Shrimali, M., Bharti, S., and Dumne, S. (2015). "Seismic response analysis of coupled building involving mr damper and elastomeric base isolation." *Ain Shams Engineering Journal*, 6(2), 457 – 470.

Silwal, B., Michael, R. J., and Ozbulut, O. E. (2015). "A superelastic viscous damper for enhanced seismic performance of steel moment frames." *Engineering Structures*, 105, 152 – 164.

Soong, T. T. and Dargush, G. F. (1997). *Passive energy dissipation systems in structural engineering*. Wiley.

Summers, P., Jacob, P., Marti, J., Bergamo, G., Dorfmann, L., Castellano, G., Poggianti, A., Karabalis, D., Silbe, H., and Triantafillou, S. (2004). "Development of new base isolation devices for application at refineries and petrochemical facilities." *13th World Conference on Earthquake Engineering, Vancouver, BC, Canada*, 1–6.

Taniwangsa, W. and Kelly, J. (1996). "Studies on seismic isolation for housing in developing regions." *Proceedings of the 11th World Conference on Earthquake Engineering, Acapulco, Mexico*.

Teramoto, T., Kitamura, H., and Ozaki, H. (1996). "Practical application of high-damping rubber

596 dampers to a slender building." *11th World Conference on Earthquake Engineering, 11WCEE*
597 *1996*, Vol. 1801.
598 Torvik, P. and Bagley, R. (1984). "On the appearance of the fractional derivative in the behavior of
599 real materials.." *Journal of Applied Mechanics, Transactions ASME*, 51(2), 294–298.
600 Vargas, R. and Bruneau, M. (2007). "Effect of supplemental viscous damping on the seismic re-
601 sponse of structural systems with metallic dampers." *Journal of Structural Engineering*, 133(10),
602 1434–1444.
603 Yu, Y., Li, Y., Li, J., and Gu, X. (2016). "A hysteresis model for dynamic behaviour of magnetorhe-
604 ological elastomer base isolator." *Smart Materials and Structures*, 25(5), 055029.

List of Tables

TABLE 1. Elastomer' Properties (Muhr 2019)

Property	**Unaged**	**Aged**
Dynamic Shear modulus (100% strain, 1Hz; MPa)	0.76	0.86
Dynamic Shear loss factor (100% strain, 1Hz)	0.52	0.5
Shear failure strain (strain rate $1s^{-1}$; %)	450	-
Tensile strength (MPa)	6.6	7.5
Tensile elongation at break	640	630
Trouser tear strength (N/mm)	6.7	-

TABLE 2. Mechanical Properties at a range of strain amplitudes, frequencies and temperatures

Temperatures	Shear Strain %	f=0.25Hz		f=0.5Hz		f=1Hz		f=2Hz		f=3Hz		f=4Hz	
		G′(MPa)	n	G′(MPa)	n	G′(MPa)	n	G′(MPa)	n	G′(MPa)	n	G′(MPa)	n
T =20°C	10	1.36	0.41	1.36	0.41	1.47	0.41	1.62	0.40	1.70	0.40	1.77	0.39
	20	1.04	0.36	1.08	0.35	1.15	0.35	1.24	0.35	1.30	0.35	1.34	0.35
	30	0.88	0.33	0.92	0.33	0.98	0.33	1.05	0.34	1.09	0.33	1.12	0.33
	40	0.81	0.34	0.84	0.33	0.89	0.33	0.95	0.33	0.98	0.33	1.01	0.33
	50	0.77	0.30	0.80	0.30	0.84	0.31	0.89	0.31	0.92	0.31	0.95	0.31
T =25°C	10	1.31	0.39	1.33	0.38	1.43	0.37	1.55	0.37	1.62	0.36	1.66	0.36
	20	1.01	0.33	1.01	0.33	1.08	0.33	1.16	0.33	1.21	0.32	1.25	0.32
	30	0.83	0.32	0.86	0.31	0.91	0.31	0.97	0.31	1.01	0.31	1.04	0.31
	40	0.75	0.30	0.77	0.30	0.82	0.30	0.86	0.31	0.89	0.30	0.92	0.30
	50	0.70	0.30	0.72	0.29	0.75	0.30	0.80	0.30	0.82	0.30	0.84	0.30
T =30°C	10	1.13	0.36	1.13	0.37	1.21	0.36	1.31	0.36	1.37	0.35	1.42	0.36
	20	0.88	0.32	0.89	0.32	0.95	0.32	1.02	0.32	1.07	0.32	1.10	0.31
	30	0.76	0.31	0.80	0.30	0.84	0.30	0.89	0.30	0.93	0.30	0.95	0.30
	40	0.67	0.29	0.71	0.28	0.75	0.29	0.79	0.29	0.82	0.29	0.84	0.29
	50	0.66	0.28	0.68	0.28	0.71	0.28	0.75	0.29	0.78	0.29	0.82	0.28
T =35°C	10	1.01	0.35	1.02	0.35	1.08	0.35	1.17	0.35	1.22	0.35	1.27	0.34
	20	0.80	0.30	0.82	0.30	0.87	0.31	0.94	0.31	0.97	0.30	1.00	0.30
	30	0.73	0.28	0.77	0.29	0.81	0.29	0.81	0.29	0.85	0.29	0.86	0.29
	40	0.64	0.28	0.67	0.28	0.70	0.28	0.75	0.29	0.77	0.28	0.79	0.28
	50	0.61	0.27	0.63	0.27	0.66	0.27	0.70	0.27	0.72	0.27	0.73	0.27

TABLE 3. MGMM Parameters under 20^{o}C

k1 (kN/mm)	**c1 (kNsec/mm)**	**k0 (N/mm)**	**c_NL(kN/((mm/sec)$^{0.374}$))**	α	
0.515	0.0151	0.107	1.585	0.374	
k_a (kN/mm)	**k_b (kN/mm)**	**u_ref (mm)**	**c_a (kNsec/mm)**	**c_b (kNsec/mm)**	**v_ref (mm/sec)**
3.741	3.613	7.966	0.902	0.190	13.468

TABLE 4. Values of γ_T for different ambient temperatures

γ_{20}	γ_{25}	γ_{30}	γ_{35}
1	0.935	0.875	0.820

TABLE 5. NRMS error (%) between MGMM and experimental data for sweep amplitude tests under a range of frequencies and temperatures

	Frequency (Hz)					
Temperature (C)	**0.25**	**0.5**	**1**	**2**	**3**	**4**
20	1.60	1.45	1.72	1.73	1.41	1.57
25	1.64	1.51	1.76	1.68	1.71	1.83
30	1.10	1.24	1.57	1.49	1.51	1.55
35	1.46	1.61	1.52	1.72	1.64	1.59

List of Figures

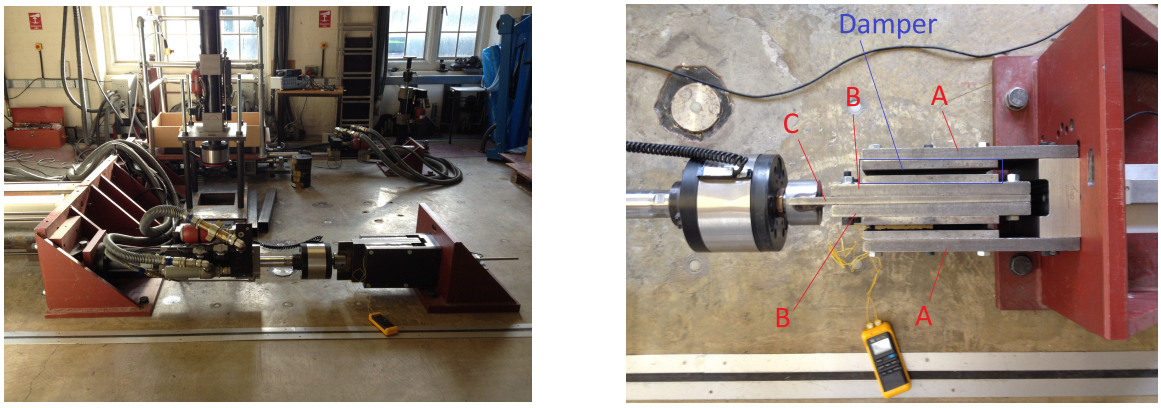

(a) **(b)**

Fig. 1. Experimental Rig

(a)

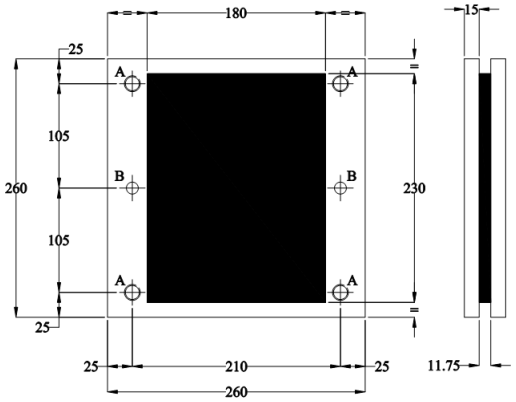

(b)

Fig. 2. Individual Damper

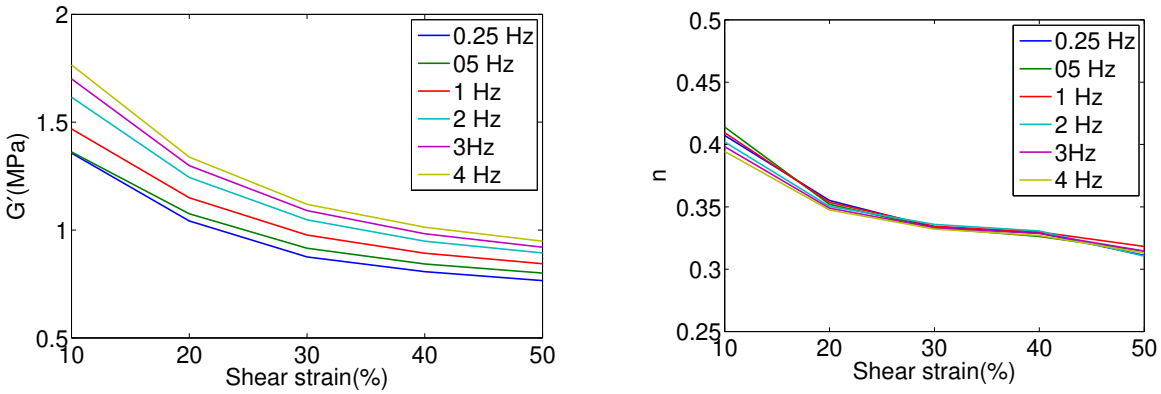

Fig. 3. Mechanical Properties evaluated from characterization tests under 20^{o}C: (a) Shear storage modulus, and (b) loss factor

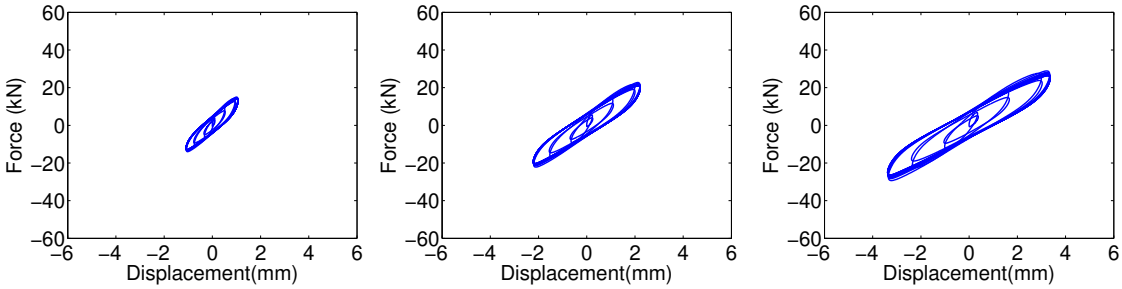

(a) 10% strain **(b)** 20% strain **(c)** 30% strain

(d) 40% strain **(e)** 50% strain

Fig. 4. ED's hysteresis loops for 2.0 Hz and 20°C

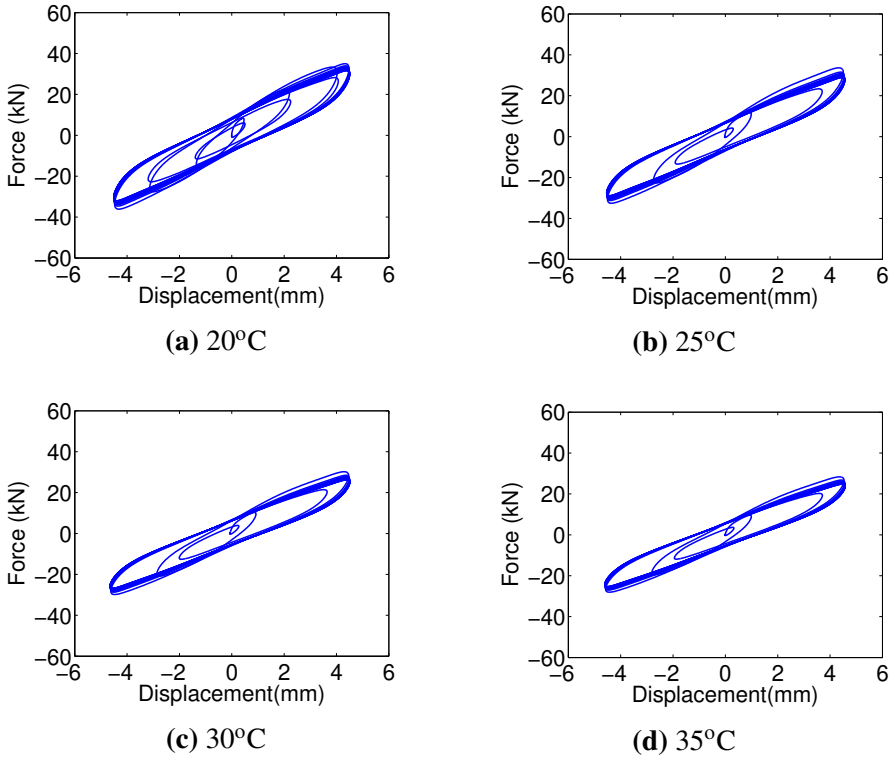

(a) 20°C **(b)** 25°C

(c) 30°C **(d)** 35°C

Fig. 5. Hysteresis loops for 2.0Hz, 40% shear strain for various temperatures

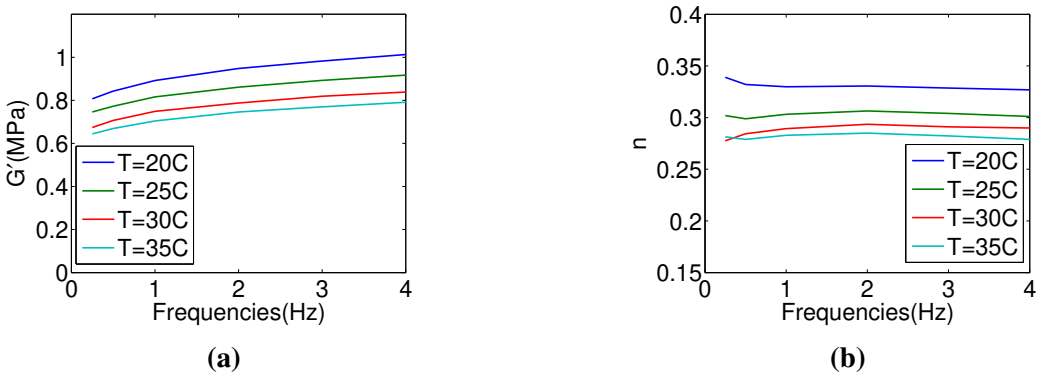

(a) **(b)**

Fig. 6. Mechanical properties from characterization tests under 40% shear strain for various temperatures

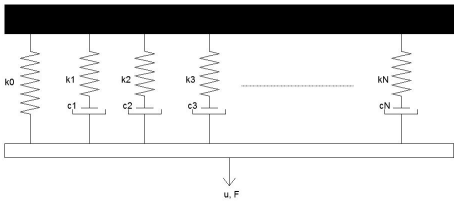

Fig. 7. Linear Generalized Maxwell Model (GMM)

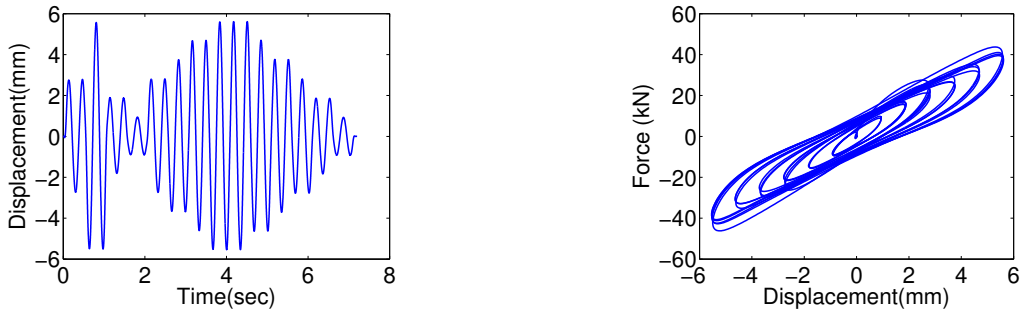

(a) **(b)**

Fig. 8. Sweep amplitude test for frequency of 3 Hz

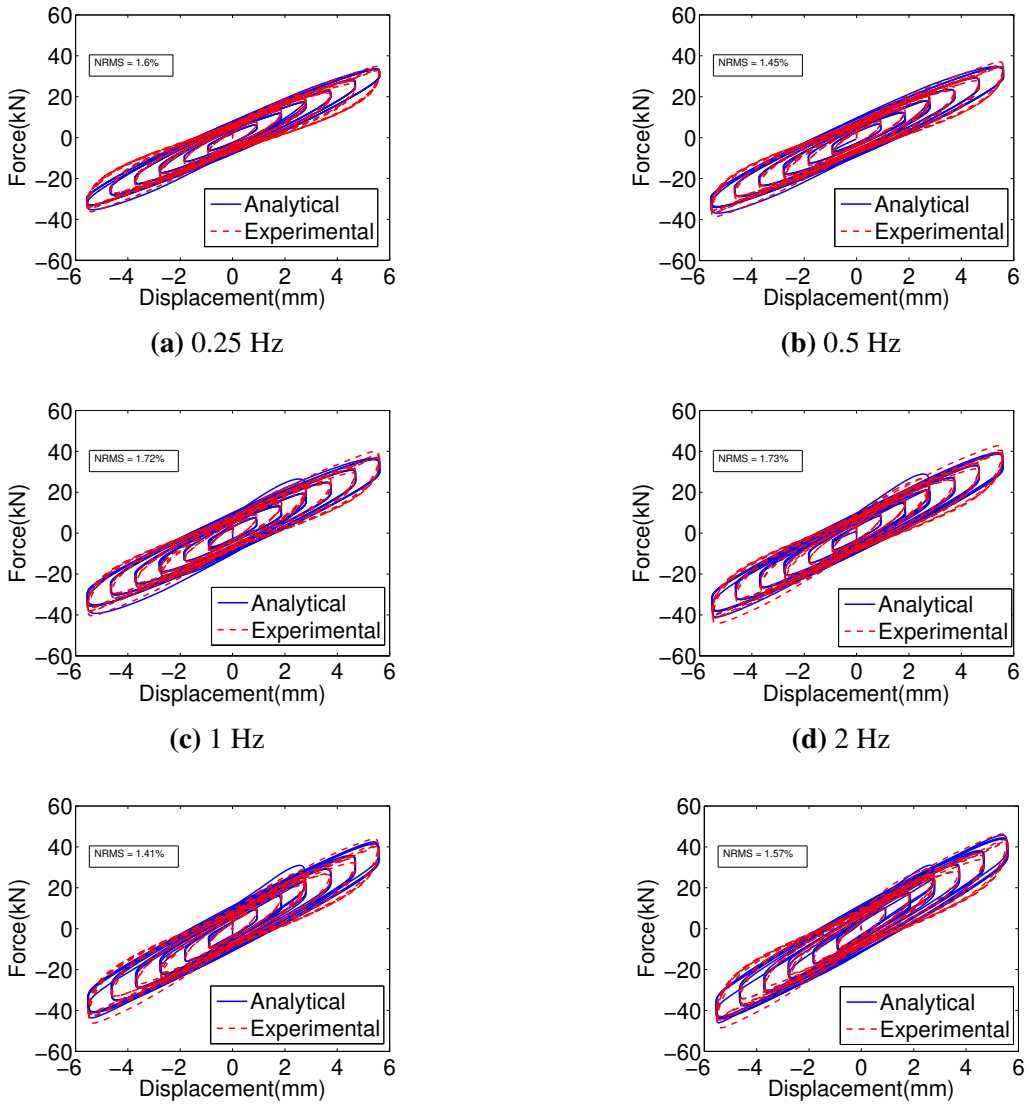

(a) 0.25 Hz **(b)** 0.5 Hz

(c) 1 Hz **(d)** 2 Hz

(e) 3 Hz **(f)** 4 Hz

Fig. 9. Comparison of force between experiments and MGMM model for sweep amplitude test under 20°C

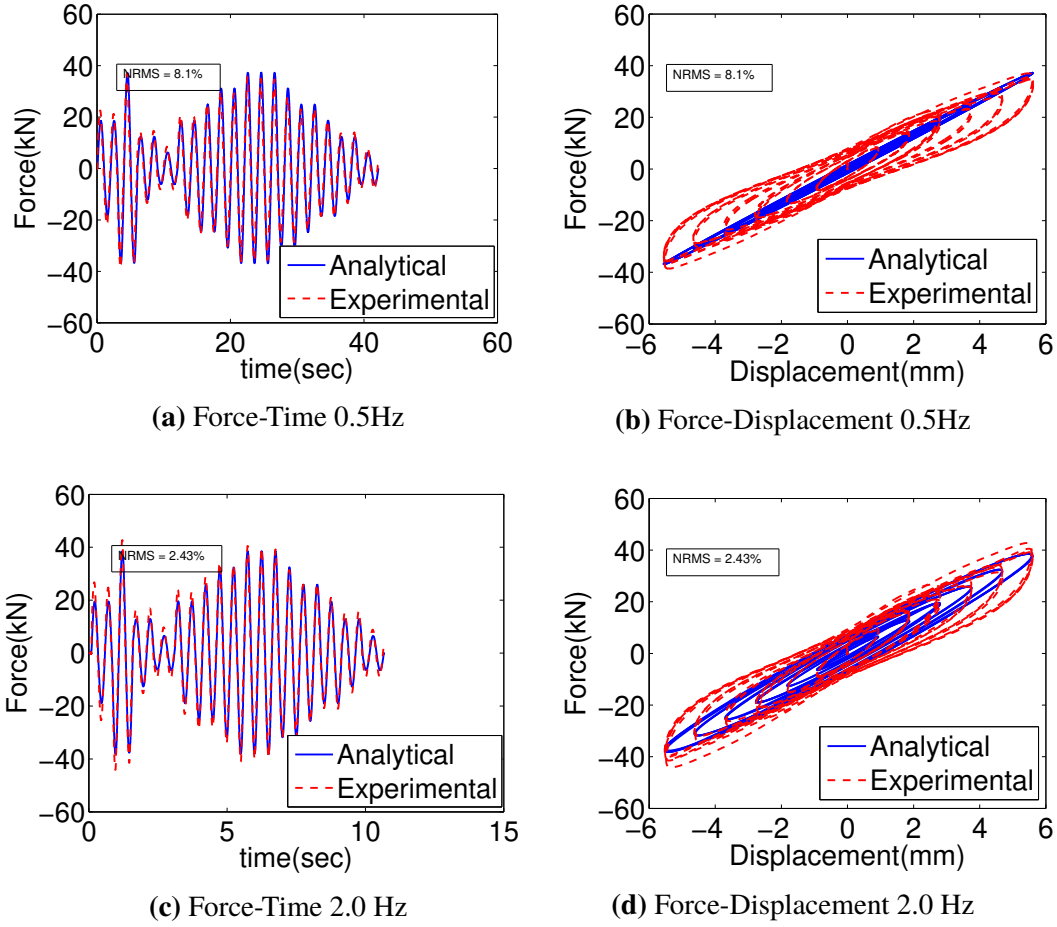

(a) Force-Time 0.5Hz

(b) Force-Displacement 0.5Hz

(c) Force-Time 2.0 Hz

(d) Force-Displacement 2.0 Hz

Fig. 10. Comparison of GMM with experimental data

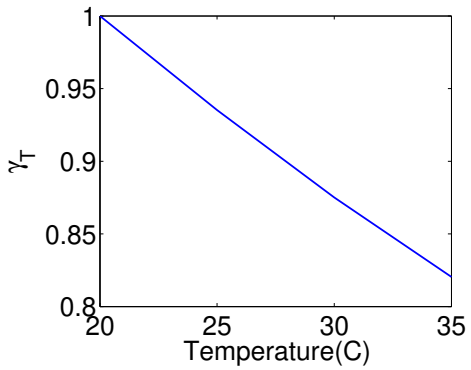

Fig. 11. Alteration of temperature parameter γ_T with different temperatures

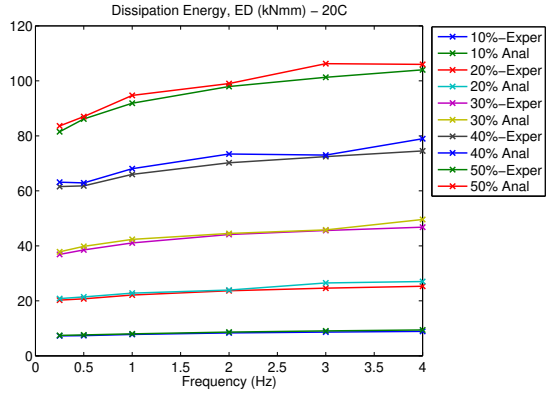

Fig. 12. Dissipation Energy Comparison for T=20^{o}C

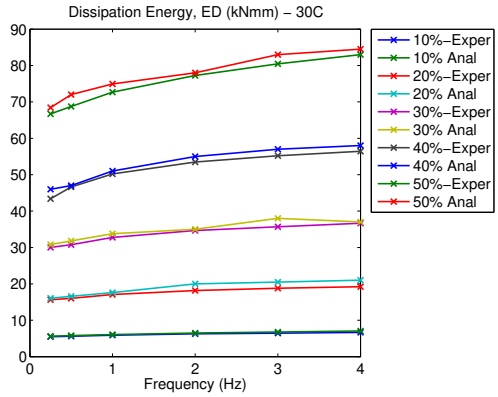

Fig. 13. Dissipation Energy Comparison for T=30^{o}C